Leading Edge Vortex Development on Pitching and Surging Airfoils: A Study of Vertical Axis Wind Turbines

R. Dunne, H.C. Tsai, T. Colonius and B.J. McKeon

Abstract Vertical axis wind turbine blades undergo dynamic stall due to the large angle of attack variation they experience during a turbine rotation. Particle image velocimetry on a pitching and surging airfoil was used to perform time resolved measurements at blade Reynolds numbers near turbine operating conditions of 10^5. These experiments were compared to simulations performed in the rotating turbine frame as well as the linear, experimental, frame at a Reynolds number of 10^3 to investigate rotational and Reynolds number effects. The flow was shown to develop similarly prior to separation, but the kinematics of vortices shed post separation were reference frame dependent.

1 Introduction

Due to their relatively smaller footprint, vertical axis wind turbines (VAWTs) can be placed in tightly spaced arrays, resulting in an increase of energy density (defined as energy per acre of land) as compared to horizontal axis wind turbines (HAWTs) which suffer from destructive interference unless well spaced [4, 6]. The vertical axis of rotation however makes the aerodynamics of VAWTs much more complicated, and as a result the efficiency of individual VAWTs is over 10 % lower than HAWTs.

R. Dunne (✉) · H.C. Tsai · T. Colonius · B.J. McKeon
California Institute of Technology, 1200 E California Blvd,
Pasadena, CA 91125, USA
e-mail: rdunne@caltech.edu

H.C. Tsai
e-mail: htsai@caltech.edu

T. Colonius
e-mail: colonius@caltech.edu

B.J. McKeon
e-mail: mckeon@caltech.edu

A. Segalini (ed.), *Proceedings of the 5th International Conference on Jets, Wakes and Separated Flows (ICJWSF2015)*,
Springer Proceedings in Physics 185, DOI 10.1007/978-3-319-30602-5_71

337595_1_En_71_Chapter ☑TYPESET ☐DISK ☐LE ☑CP Disp.:6/5/2016 Pages: 8 Layout: T1-Standard

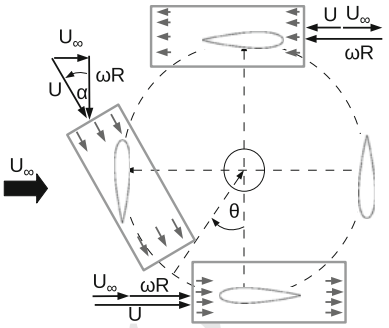

Fig. 1 *Top* view of a VAWT, showing the conditions encountered by a single blade at four angles during VAWT rotation. Wind speed U_∞, effective velocity U, blade velocity ωR. Experimental field of view shown by *grey boxes* (not to scale)

The turbines considered in this study are similar to the commercial 1.2 kW Windspire turbines used by Kinzel et al. [6] and rotate at a tip speed ratio $\eta = \frac{\omega R}{U_\infty} = 2$ where R is the radius of the turbine, U_∞ is the wind velocity and ω is the turbine rotation rate. A schematic of a VAWT is shown in Fig. 1 demonstrating angle of attack α and effective velocity U. Only blades in the upstream half of the turbine cycle ($0° < \theta < 180°$) will be considered here as it has been shown that blades in the downstream half of the turbine rotation produce negligible power when compared to the upstream blades [5].

Dynamic stall on a representative one-bladed VAWT has been studied experimentally in the rotating frame at a limited number of angular positions at Reynolds numbers near operating conditions and tip speed ratios of 2, 3 and 4 by Ferreira et al. [7]. The growth of leading edge and trailing edge vorticity was analysed at several positions around the turbine cycle and the total vortex circulation was shown to grow until the vortex is shed at the point of dynamic stall. In order to capture the evolution of vortical structure, time resolved velocity measurements of a pitching and surging airfoil as a surrogate for a VAWT blade were performed by Dunne and McKeon [3]. They developed a simple 5 mode model using the dynamic mode decomposition that captures LEV development and the dynamic stall process. Computations by Tsai and Colonius at similar conditions but a much lower Reynolds number investigated the effect of the Coriolis force by comparing the pitch/surge motion of Dunne and McKeon to the rotating frame of the turbine [8].

This paper combines experiment and simulation to investigate the effect of Reynolds number and the rotating reference frame on the dynamic stall process. Experimental data in the equivalent planar pitch/surge reference frame, hereafter **EPM**^{E}, provides measurements at Reynolds numbers characteristic of full scale VAWTs at the expense of neglecting the Coriolis effect. Direct numerical simulations provide comparisons at low Reynolds number of the equivalent planar motion (**EPM**^{C}) and VAWT frame including Coriolis forces (**VAWT**^{C}). The rationale for looking at the two-dimensional, low Reynolds number regime in computation is that a much larger parameter space can be considered, and effects of blade rotation, pitch, surge, and so on can be isolated independently from uncertainties associated with turbulence models. Of course, the disadvantage of this approach is computations and

337595_1_En_71_Chapter ☑TYPESET ☐DISK ☐LE ☑CP Disp.:6/5/2016 Pages: 8 Layout: T1-Standard

experiments can only be compared qualitatively. In this paper, the different techniques are used to model a region of the parameter space corresponding to VAWT operation. The **EPM**^{C} and **VAWT**^{C} results offer a self-consistent investigation of the influence of rotation within an immersed boundary condition simulation, while a comparison of **EPM**^{C} and **EPM**^{E} cases isolate Reynolds number effects and the differences between experiment and simulation, including all considerations of relevant boundary conditions, which are assumed to be small.

2 Experimental and Computational Methods

Conditions for experiment were chosen to closely match those of a representative $\eta = 2$ vertical axis wind turbine using a NACA 0018 airfoil. Sinusoidal pitch between $\alpha_\pm = -30$ and 30° about the leading edge (where the subscript $\pm$ indicates pitch up $+$ and down $-$) and surge of $\frac{U_{max}-U_{min}}{\bar{U}} = 0.9$ at reduced frequency $k = \frac{\omega c}{2\eta U_\infty} = 0.12$ were selected to mimic the frequency, angle of attack and velocity variation of the turbine consisting of slightly skewed sinusoids at with similar magnitude ($-30° \leq \alpha \leq 30°$ and $\frac{U_{max}-U_{min}}{\bar{U}} = 1$). Experimental Reynolds numbers of 10^5 match the physical turbine in the American Wind Energy Association (AWEA) national average wind velocity of 5 m s^{-1} [1].

This field of view shown by grey boxes in Fig. 1 is fixed in the lab frame, and the airfoil pitches/surges inside it to achieve the desired angle of attack and velocity. Multiple experiments were performed using particle image velocimetry in overlapping forward and aft fields of view to measure the velocity field over the entire airfoil motion, then ensamble averaged and knit together to form a composite field of view shown in the airfoil reference frame by white lines in Fig. 2. Further detail of the experimental setup including hardware, PIV setup, and processing details can be found in Dunne and McKeon 2015 [3].

In the computation, the chord Reynolds numbers were limited to $Re \leq 1500$, but both the experimental, pitch/surge frame (**EPM**^{C}), and the full turbine frame (**VAWT**^{C}) including Coriolis forces were investigated. Computations were performed on a single NACA 0018 airfoil using the immersed boundary projection method developed by Colonius and Taira [2] to compute two-dimensional incompressible flows in an airfoil-fixed reference frame. To account for the non-inertial reference frame appropriate forces were added to the momentum equation. Further details, including a discussion of the verification and validation of the algorithm, can be found in Tsai and Colonius 2015 [8].

3 Results

An isocontour of the spanwise vorticity colored by the velocity magnitude (scaled by the maximum velocity) of the phase averaged velocity fields from experiment (**EPM**^{C}) is shown in Fig. 2 where time is extruded along the Z axis for two periods of the airfoil motion. The period begins at point A, $\theta = 0°$, with maximum freestream velocity (maximum surge) and zero angle of attack. At this point the flow is attached to the airfoil. As the airfoil pitches up and decelerates it separates at point B ($\alpha_+ \sim 25°$), well beyond the static stall point of $\alpha_{ss} \sim 11°$, forming a separated shear layer indicated by the vorticity isocontour lifting away from the airfoil. Finally the airfoil pitches down to point C near $\alpha_- = 0$ when the flow reattaches to the airfoil. From C to A', at the start of the second cycle, the airfoil is at negative angle of attack and the vorticity indicates the shear due to the no-slip condition on the pressure side of airfoil surface. The dynamic stall process including leading edge vortex (LEV) growth is described in Dunne and McKeon 2015 [3].

The vorticity is plotted in the lab frame at various phases of the airfoil motion in Fig. 3 for all three cases. The lower Reynolds numbers in the simulation result in much more coherent vortices appearing at all angles of attack. Furthermore the experimental data is an ensemble average of multiple experiments, and as such the coherent vortex shedding apparent at $\alpha_+ = 0°$ that is not exactly coupled to the airfoil phase is smeared out in experimental results. This phase averaging also significantly weakens the positive (counter-clockwise) vorticity at the airfoil surface due to the interaction of the recirculation region and the airfoil surface after separation, and as such is only apparent in the computations.

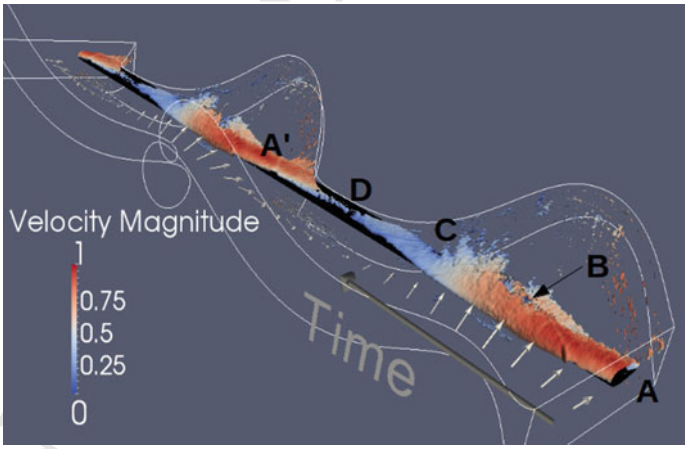

Fig. 2 Vorticity isocontour *colored* by scaled velocity magnitude ($\frac{\sqrt{u^2+v^2}}{max(\sqrt{u^2+v^2})}$). Two periods shown. *Arrows* indicate incoming angle of attack variation. Points A, A' correspond to $\alpha = 0$, B to separation location, and C to reattachment D to minimum angle of attack. *White lines* show field of view in airfoil fixed frame

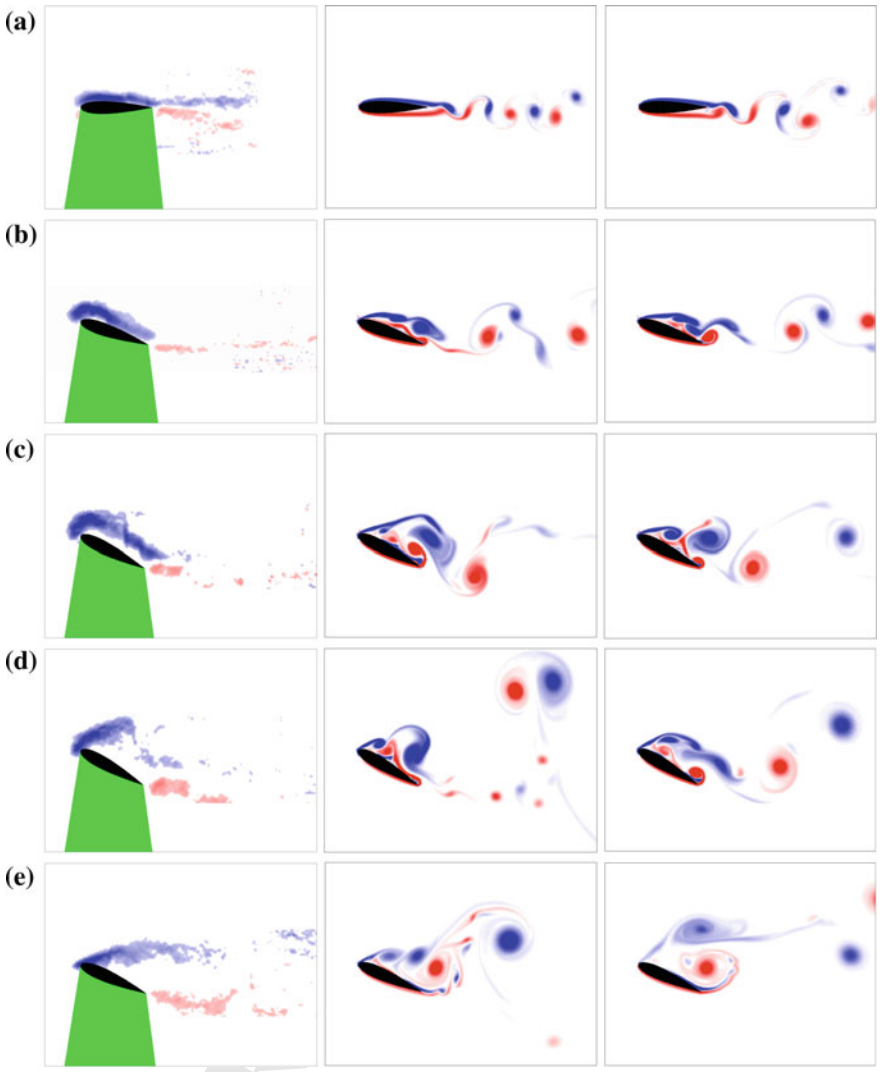

Fig. 3 Vorticity contours from experiment $\mathbf{EPM}^E$ (*left*) and computation of the pitch/surge motion $\mathbf{EPM}^C$, (*middle*) and the computation of the $\mathbf{VAWT}^C$, (*right*). *Red* and *blue* contours indicate positive and negative vorticity respectively and *green* area indicates the PIV laser *shadow*. **a** $\theta = 0°, \alpha_+ = 0°$, **b** $\theta = 60°, \alpha_+ = 19.1°$, **c** $\theta = 90°, \alpha_+ = 26.6°$, **d** $\theta = 120°, \alpha = 30°$, **e** $\theta = 150°, \alpha_- = 23.8°$

Apart from these Reynolds number and experimental differences the flow evolution is similar between the three cases and qualitatively similar to the experiments of Ferreira et al. [7]. Initially at $\alpha_+ = 0°$ the flow is attached and a symmetrical wake can be seen behind the airfoil. At $\alpha_+ = 19°$ a leading edge vortex begins to form,

visible as a distinct structure in computation and indicated by increased intensity in experiment. At this point the flow remains primarily attached without a large reversed region behind the airfoil. At $\alpha_+ = 27°$ the LEV appears even stronger in experiment, and the flow has just begun to separate, in both computations however the LEV has moved downstream, indicating flow separation occurring slightly earlier at low Reynolds number. At maximum $\alpha = 30°$ the flow is fully separated in both experiment and computation with a shear layer between stagnant and freestream flow visible in experiment, and large scale vortex shedding from leading and trailing edge continuing in the computation, while the initial leading and trailing edge vortices, apparent further downstream in computation corresponding to the slightly earlier separation point. Slight differences can be seen in the trajectories of the shed vortices between the EPM and VAWT frames, with a vortex pair moving up away from the airfoil in the linear frame and, two distinct but opposite vortices moving downstream in the rotating one. Finally on pitch down at $\alpha_- = 24°$ the VAWT shows two vortices captured by the airfoil, while in the linear frame vortices can be seen to shed from the leading and trailing edges. More detail of this wake capture phenomenon can be found in Tsai and Colonius 2015 [8].

Vorticity contours are plotted in the turbine reference frame for both the experiment and the VAWT simulation at various points in the airfoil cycle in Fig. 4. Similar to Fig. 3 the VAWT computation shows more coherent vortices as to be expected due to the lower Reynolds number. The effect of the experimental and turbine reference frame can be seen clearly, as the vortices in the airfoil reference frame convect from

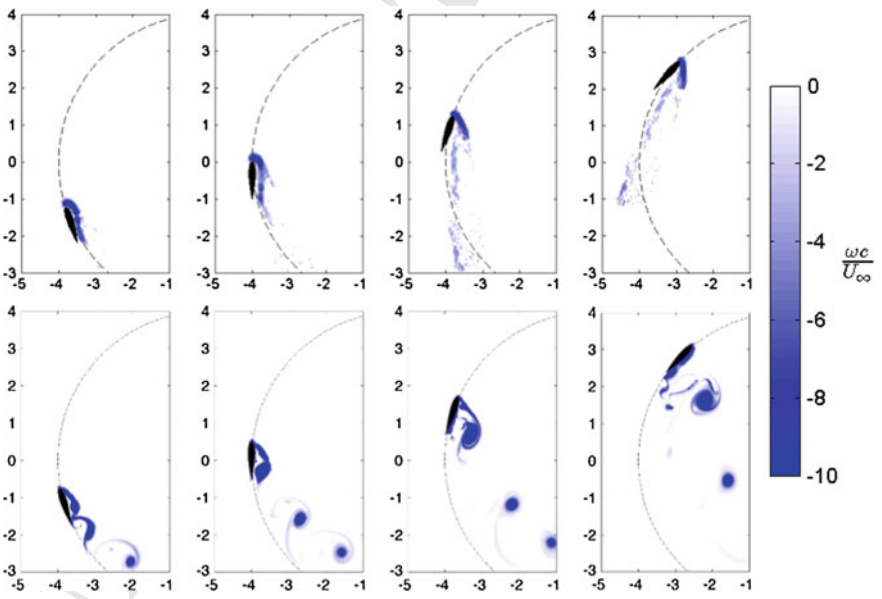

Fig. 4 *Clockwise* vorticity contours from experiment $\mathbf{EPM}^E$ (*top*) and VAWT computation $\mathbf{VAWT}^C$ (*bottom*) at $\theta = 70°$, 90°, 108° and 133° respectively from *left* to *right*

left to right with the turbine relative freestream, while the vortices in the experiment convect behind the airfoil with the blade relative free stream. However, at the blade level and immediately behind it, agreement is good.

4 Conclusion

Dynamic stall, flow separation and leading edge vortex development were studied to analyse the flow experienced by vertical axis wind turbine blades. The VAWT flow was modeled in two different ways: using experiments on a blade undergoing linear motion and by simulation of both rotating and linearly traversing blades using an immersed boundary condition code. A 'pitch/surge' model of the flow was used experimentally to perform time resolved measurements at full scale turbine blade Reynolds numbers, at the expense of a change of reference frame, which excluded the rotational, Coriolis force. The high Reynolds numbers of physical turbines were not simulated in computation, however both experimental (pitch/surge) and turbine reference frames were calculated such that self-consistent comparisons across all three conditions can be made. As such this dual approach provides insight into the evolution of vortical structure and separation on VAWT blades as well as understanding of the effect of Reynolds number and Coriolis forces.

Acknowledgments This work was supported by the Gordon and Betty Moore Foundation through grant GBMF#2645 to the California Institute of Technology.

References

1. S. Brent, AWEA standard update, in *2009 Small Wind Turbine Testing Workshop. National Wind Technology Center (NWTC)* (2009)
2. T. Colonius, K. Taira, A fast immersed boundary method using a nullspace approach and multi-domain far-field boundary conditions. Comput. Methods Appl. Mech. Eng. **197**(25–28), 2131–2146 (2008)
3. R. Dunne, B. McKeon, Dynamic stall on a pitching and surging airfoil. Exp. Fluids **56**:157 (2015). (see also AIAA Paper 2015-3142)
4. E. Hau, *Wind Turbines: Fundamentals, Technologies, Application, Economics* (Springer, Berlin, 2013)
5. M. Islam, D.S.K. Ting, A. Fartaj, Desirable airfoil features for smaller-capacity straight-bladed VAWT. Wind Eng. **31**(3), 165–196 (2007)
6. M. Kinzel, Q. Mulligan, J.O. Dabiri, Energy exchange in an array of vertical-axis wind turbines. J. Turb. **13**(38), 1–13 (2012)
7. C. Simão Ferreira, G. van Kuik, G. van Bussel, F. Scarano, Visualization by PIV of dynamic stall on a vertical axis wind turbine. Exp. Fluids **46**(1), 97–108 (2009)
8. H.C. Tsai, T. Colonius, Coriolis effect on dynamic stall in a vertical axis wind turbine. AIAA J. (to appear; see also AIAA Paper 2015-3140)

Replace with: Tsai, H.C. and Colonius, T., "Coriolis effect on dynamic stall in a vertical axis wind turbine," AIAA Journal, Vol 54, No.1, 2016, pp. 216-226

Author Queries

Chapter 71

Query Refs.	Details Required	Author's response
	No queries.	

MARKED PROOF

Please correct and return this set

Please use the proof correction marks shown below for all alterations and corrections. If you wish to return your proof by fax you should ensure that all amendments are written clearly in dark ink and are made well within the page margins.

Instruction to printer	*Textual mark*	*Marginal mark*
Leave unchanged	··· under matter to remain	
Insert in text the matter indicated in the margin		New matter followed by or
Delete	through single character, rule or underline or through all characters to be deleted	or
Substitute character or substitute part of one or more word(s)	through letter or through characters	new character or new characters
Change to italics	under matter to be changed	
Change to capitals	under matter to be changed	
Change to small capitals	under matter to be changed	
Change to bold type	under matter to be changed	
Change to bold italic	under matter to be changed	
Change to lower case	Encircle matter to be changed	
Change italic to upright type	(As above)	
Change bold to non-bold type	(As above)	
Insert 'superior' character	through character or where required	or under character e.g. or
Insert 'inferior' character	(As above)	over character e.g.
Insert full stop	(As above)	
Insert comma	(As above)	
Insert single quotation marks	(As above)	or and/or or
Insert double quotation marks	(As above)	or and/or or
Insert hyphen	(As above)	
Start new paragraph		
No new paragraph		
Transpose		
Close up	linking characters	
Insert or substitute space between characters or words	through character or where required	
Reduce space between characters or words	between characters or words affected	